Molecular Dynamics Simulation Study of Parallel Telomeric DNA Quadruplex at Different Ionic Strengths. Evaluation of Water and Ion Models.

Matúš Rebič,[*,†,‡,¶,§] Aatto Laaksonen,[†,¶,∥,⊥] Jiří Šponer,[#,@] Jozef Uličný,[§,‡] and Francesca Mocci[*,⊥,†,¶]

Division of Physical Chemistry, Department of Materials and Environmental Chemistry, Arrhenius Laboratory, Stockholm University, 10691 Stockholm, Sweden, Department of Biophysics, Faculty of Science, P. J. Šafárik University, Jesenná 5, 041 54 Košice, Slovakia, Science for Life Laboratory (SciLifelab), 17121 Solna, Sweden, Centre for Multimodal Imaging (CMI), Department of Biophysics, Institute of physics, P. J. Šafárik University, Jesenná 5, 041 54 Košice, Slovakia, Stellenbosch Institute of Advanced Study (STIAS), Wallenberg Research Centre at Stellenbosch University, 7600 Stellenbosch, South Africa, Department of Chemical and Geological Sciences, University of Cagliari, I-09042 Monserrato, Italy, Institute of Biophysics, Academy of Sciences of the Czech Republic (AVČR), Kralovopolska 135, 612 65 Brno, Czech Republic, and Central European Institute of Technology (CEITEC), Campus Bohunice, Kamenice 5, 625 00 Brno, Czech Republic

E-mail: matus.rebic@mmk.su.se; fmocci@unica.it

Phone: +39 070 675 4390. Fax: +39 070 675 4388

Abstract

Most Molecular Dynamics simulations of DNA quadruplexes have been performed at minimal salt condition using the Åqvist potential parameters for the cation with the TIP3P water model. Recently this combination of parameters has been reported to give problems for the stability of quadruplex DNA, especially caused by the ion interactions inside or nearby the quadruplex channel. Here we verify how the choice of ion parameters and water model can affect the quadruplex structural stability and the interactions with the ions outside the channel. We have performed a series of MD simulations of the human full-parallel telomeric quadruplex by neutralizing its negative charge with K+ ions. Three combinations of different cation potential parameters and water models have been used : (a) Åqvist ion parameters, TIP3P water model (b) Joung and Cheatham ion parameters, TIP3P water model and (c) Joung and Cheatham ion parameters, TIP4P$_{ew}$ water model. For the combinations (b) and (c) the effect of the ionic strength has been evaluated by adding increasing amounts of KCl salt (50, 100, 200 mM). Two independent simulations using the Åqvist parameters with the TIP3P model show that this combination is clearly less suited for the studied quadruplex with K+ as counter ions. In both simulations one ion escapes from the channel, followed by significant deformation of the structure leading to deviating conformation compared to that in the reference crystallographic data. For the other combinations of ion and water potentials no tendency is observed for the channel ions to escape from the quadruplex channel. In addition, the internal mobility of the three loops, the torsion angles and the counter ion affinity have been investigated at varied salt concentrations. In summary, the selection of ion and water models is crucial as it can affect both the structure and the dynamics as well as the interactions of the quadruplex with its counter ions. The

*To whom correspondence should be addressed
†Stockholm University
‡P. J. Šafárik University
¶SciLifelab
§CMI
‖STIAS
⊥University of Cagliari
#AVČR
@CEITEC

results obtained with the TIP4P$_{ew}$ are found to be closest to the experimental data at all the studied ion concentrations.

1 Introduction

The chromosomal DNA of the human genome contains guanine-rich hexanucleotide tandems $d(TTAGGG)_n$,[1] which can form non-canonical DNA structures called G-quadruplexes. Among unconventional DNA structures, quadruplexes seem to have most biological implications.[2–5] In a quadruplex structure four guanine bases are connected within a plane through a network of Hoogsteen hydrogen bonds forming a stable G-tetrad. Additionally, the whole system is stabilized by monovalent cations located between two adjacent G-tetrads.[6–8] The relative orientation of the backbone chains, to which the guanines are bound, allows formation of three different basic classes of topologies,[9] namely parallel,[10] anti-parallel[11] and hybrid.[12] Until 2015 only right handed conformations were known to exist; recently it has been shown experimentally that even left handed quadruplexes can be formed for specific sequences.[13]

Various force fields are used for simulating nucleic acids, and among them the two most frequently used and tested are the second generation Amber force field derived by the Cornell *et al.*[14] and CHARMM force field derived from the C27 parameter set.[15] While it is known that the CHARMM force field describes the B-DNA well, systematic or more extensive simulation studies of non-canonical DNAs do not exist to date.[16] The limited MD investigation of G-quadruplex with CHARMM force field by Fardna *et al.* does not provide fully satisfactory results for such non-canonical DNA.[17] Better results have been obtained with the Amber force field, which is the force field extensively used so far to simulate G-quadruplexes. A variety of ion parameters and water models have been used together with Amber force field for quadruplexes, similarly to what have been observed in the simulations of canonical DNA duplexes.[18] In Table 1 we have summarized the ion potential parameters and water models used in recent Molecular Dynamics (MD) simulations of quadruplexes. We limit the data

taken from simulations performed after 2009 and using the Amber Parmbsc0[19] force field for the quadruplex. From Table 1 we can see that in many recent simulations the TIP3P water model[20] and the Amber adapted Åqvist's parameters[21] for the ions have been used. This particular choice of water and ion parameters has, however, reported to cause departures of K^+ cations from the highly electronegative channel, located along the axis of the G-tetrads. This is an artefact due to the short range repulsion term of the ion Lennard-Jones potential being too repulsive, as described by Fadrná *et al.*[17] and by Konstantinos *et al.*[22] One possible way to preserve the correct coordination of the K+ ions inside the channel is to use slightly smaller ion radii parameters, as suggested by Hazel *et al.*[23] An additional problem of the Amber adapted Åqvist's parameters occurs at non zero salt concentration simulations, where a non-physical formation of KCl aggregates has been observed using the default parameters of the Amber software.[24,25]

A new set of parameters for ions has been developed by Joung and Cheatham[40] in order to improve their bulk behaviour in water solution, and they are now commonly used by the nucleic acid simulation community.[18] As far as quadruplexes are concerned, MD simulations with these parameters have already been tested in combination of TIP3P water model.[17] These ion parameters have been optimized also for the $TIP4P_{ew}$[46] model, but not controlled for quadruplexes so far. Even small differences in water models and ion parameters can influence the interaction of nucleic acids with water, and local phenomena can easily spread over large portion of the DNA structure and flaw the final MD simulation results. The effects on RNA duplex structures of the explicit water models used in MD simulations have been recently addressed by Kührová *et al.*;[47] they found that helical parameters such as roll, inclination and slide are affected by the water model. Such a structural effect was found to be due to water bridging between hydroxylic groups belonging to opposite nucleic acid chains, which in turn is due to a different capability of the used water model to describe more complex topologies. Krepl *et al.*[33] pointed out differences between the TIP3P and TIP5P water model usage on the anti-parallel DNA quadruplex, where the pucker degradation of

Table 1: Overview of the MD simulations of quadruplex DNA using the Parmbsc0[19] force field reported after 2009. Empty space in the table indicates the use of the same parameters as specified in the row above. [a]Counter ion type. [b]Counter ion parameters with the following abbreviations: AA: AMBER-adapted Åqvist;[21] JC: Joung and Cheatham;[40] SD: Smith and Dang;[41] DK: Dang and Kollman;[42] H: Hazel *et al.*[23] [c]Counterions concentration. [d]Trajectory length. [e]Water model: TIP3P;[20] SPC/E;[43,44] TIP4P;[20] TIP5P.[45] [f]Modified structures. [g]Various combinations of these three structures have been used to build up different higher quadruplex hybrids. [h]Unfolding study.

Structure (PDB id)	CI [a]	CIp [b]	CIc [c] *(mM)*	Tr [d] *(ns)*	Water [e] model	Group	Year	Ref.
1JRN	Na^+	AA	0	50	TIP3P	Fadrná *et al.*	2009	[17]
	K^+	H	0					
		DK	0					
	KCl		200					
	K^+				SPC/E			
		JC	0		TIP3P			
	KCl		200					
1KF1	Na^+	AA	0	40	TIP3P			
	K^+	DK		50				
	KCl		300					
143D, 2HY9	K^+	AA	0	50	TIP3P	Li *et al.*	2010	[26]
1KF1, 156D								
1XAV[f]	K^+	AA	0	35	TIP3P	Li *et al.*	2010	[27]
2HY9, 2JPZ	K^+	AA	0	10	TIP3P	Petraccone *et al.*	2010	[28]
1KF1[g]								
				50		Petraccone *et al.*	2011	[29]
2GKU, 1JPQ, 139B	K^+	JC	0	10	TIP3P	Cang *et al.*	2011	[30]
148D (15-TBA)	NaCl	AA	150	1000	TIP4P	Reshetnikov *et al.*	2011	[31]
	KCl							
2JT7	Na^+	AA	0	10	TIP3P	Li *et al.*	2012	[32]
2GWQ	Na^+	AA	0	200	TIP3P	Krepl *et al.*	2012	[33]
				100	TIP5P			
	K^+	DK		200	SPC/E			
	KCl	SD	200					
143D, 2GKU	K^+	AA	0	1000	TIP3P	Zhu *et al.*	2013	[34]
1KF1	K^+	H	0	1500	TIP3P	Islam *et al.*	2013	[35]
1JRN	K^+	JC	0	50	TIP3P	Song *et al.*	2013	[36]
2GWQ	Na^+	AA	0	500	TIP3P	Zgarbová *et al.*	2013	[37]
CEB1	K^+	AA	0	200	TIP3P	Adrian *et al.*	2014	[38]
1KF1, 2HY9, 143D[h]	K^+	AA	0	50	TIP3P	Bergues-Pupo *et al.*	2015	[39]

the inner-tetrads has been mitigated due to the choice of particular water model. Since it is not clear how different ion parameters and water models might affect the simulation results concerning the complicated DNA quadruplexes and their specific interaction with ions, it is necessary to verify the effect of different combinations with the aim to extract some guidelines. Also the effect of salt concentration, which has rarely been considered in simulations of quadruplexes,[17] is still to be assessed.

In this paper we address the following questions: How is the structure of the quadruplex affected by the chosen ion and water models? How are the interactions with the ions outside the channel affected by the chosen parameters? Does the variation of the ionic strength affect the quadruplex structure? To answer these questions we have performed nine 500 ns long MD simulations of the full parallel human telomeric quadruplex structure (PDB id 1KF1[10]) in water with potassium counter ions. In all simulations the DNA quadruplex force field parameters was the same (Amber Parmbsc0), but the water and ion models were changed according to the scheme shown in Table 2. Also the ionic strength was varied, starting from minimal salt conditions and adding KCl to reach salt concentration values steps of 50, 100 or 200 mM.

Table 2: Ion potential parameters used in the MD simulations presented in this paper. Empty space in the table indicates equality to the previous one in the same column. [a]Counter ion parameters with the following abbreviations: AA: AMBER-adapted Åqvist;[21] JC: Joung and Cheatham[40] [b]Water model: 3P: TIP3P;[20] 4P: TIP4P$_{ew}$[46] [c]Lennard Jones parameters for counter ions.

				LJp [c]	
	CIp [a]	W [b]		σ *(nm)*	ε *(KJ/mol)*
Set 1	AA	3P	K^+	$4.736\ 10^{-1}$	$1.372\ 10^{-3}$
Set 2	JC		K^+	$3.038\ 10^{-1}$	$8.104\ 10^{-1}$
			Cl^-	$4.478\ 10^{-1}$	$1.489\ 10^{-1}$
Set 3		4P	K^+	$2.833\ 10^{-1}$	$1.169\ 10^{-0}$
			Cl^-	$4.918\ 10^{-1}$	$4.879\ 10^{-2}$

2 Methods

As a telomeric quadruplex we have chosen the human full parallel structure with the sequence $d[AG_3(T_2AG_3)_3]$, PDB id 1KF1, schematically drawn in Figure 1. The crystal structure of this intramolecular quadruplex[10] has been used as a starting geometry for MD simulations in water solution. The nucleic acid negative net charge was neutralized with K^+ cations, two of them were initially placed inside the channel along the axis of G-tetrads in the same

positions detected in the X-ray structure. This structure contains three G-tetrads formed in a full parallel G-strands arrangement, with three propeller thymine - thymine - adenine loops on the side of the quadruplex guanine core, linking the bottom and upper G-tetrads together; beside the loops a single flanking adenine is present at the beginning of this sequence. In all of the loops of the crystal structure the adenine is inserted between the two preceding thymines and is stacked with the first thymine in the 5' $\rightarrow$ 3' direction, while the thymine, adjacent to the adenine, is not stacked with any of the bases.

The all-atom MD simulations were performed with the GROMACS software[48–50] using the Parmbsc0[19] version of the Amber parm99 force field, found suitable for simulations of non-canonical nucleic acids.[33] The DNA quadruplex shown in Figure 1 was initially centred in a cubic periodic box, with the walls placed at least 15 Å from any of the solute atoms, and filled with TIP3P[20] or TIP4P$_{ew}$[46] water molecules. The temperature was set to 298 K, and kept constant using the velocity rescale thermostat with a stochastic term[51] under 0.1 ps rescaling factor. All bonds with hydrogen atoms were constrained by the LINCS algorithm[52] and the integration time step was set to 2 fs. The electrostatic interactions were treated using the particle mesh Ewald summation method (PME)[53] with a cut-off 13 Å. The same cut-off was applied even for short-range Lennard-Jones interactions. Coordinates have been collected in trajectory files every 10 ps.

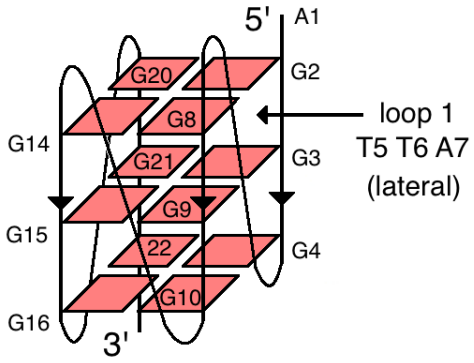

Figure 1: Schematic representation of the full parallel human telomeric 1KF1 quadruplex structure.

Each system has undergone the same equilibration process under NVT conditions and 1 fs integration time step: 100 ps MD simulations with frozen DNA and counter ions followed by 100 ps MD where the constraints on the counter ions were removed; several rounds of energy minimization each followed by 25 ps MD simulation with restrained DNA (the restraints were slowly decreased from 500 $kcal$ to zero); 100 ps MD simulation without restraints. An additional 200 ps under NPT condition with isotropic Parrinello-Rahman barostat[54,55] under 2 ps period of pressure fluctuations at equilibrium was performed to complete the equilibration stage. 500 ns trajectory of production were obtained for each system.

Trajectory processing and most of the analysis have been performed using the Gromacs Tools and computed over the last 300 ns of MD simulations. In order to decrease the clutter and to increase the clarity in root mean square deviation (RMSD) plots, we have represented every 5 ns of trajectory by a single point indicating the average value. Radial distribution functions (RDFs) were calculated using the software package MagiC.[56] To compare torsion angles between different sets we have created a convenient wheel representation, which allows a compact visualization of all of them in an arrangement from α (middle circle) to χ (edge circle) as a single plot. In addition, the color intensity reflects the percentage of occupation of a given torsion angle values during the MD, with 15° cluster resolution. All torsion angle calculations have been done using a simple in-house software, inspired by representation from the Do X3dna package.[57] The spatial distribution functions (SDFs) were calculated with the software Spatial of Gromacs Tools and presented in gaussian cube format. SDF were calculated on grid volumes of 0.125 $Å^3$ and displayed around the average structure, calculated over the same time period as the SDF. Images of the SDFs were created using the VMD software.[58]

3 Results & Discussion

The results with discussion are organized in two main sections: comparison between different simulation parameter sets (section 3.1) and comparison between simulations performed at different salt concentrations (section 3.2).

3.1 Comparison between different simulation parameter sets

3.1.1 Root mean square deviations

Set 1: AA ion parameters / TIP3P water model Already in the beginning of the simulation (around 15 ns) one of the K^+ cations exited from the electronegative quadruplex channel, coordinating to the external side of the channel's rim. The ion is kept stable in that position by the interaction with the adenine base A1, which stacks over the guanine of the tetrads, and after some time also by the interaction with another adenine from a loop (A13). At around 50 ns of simulation, a water molecule triggers the departure of the cation from the rim, and in the following 400 ps a few water molecules occupy the same position until one enters the channels, where it is kept for about 8 ns. After the water exits from the channel one ion from the channel rim moves in and out during several ns, before it occupies the coordination site between two G-tetrads. A detailed description of the mechanism is given in the Supporting material, section S9. Such ion exchange mechanism is different from those previously reported. Inspection of the RMSDs (Figure 2) shows that the exit of the ion from the channel has a clear effect on the structure: the RMSD increases from nearly 0.2 to nearly 0.4 Å. The pairwise-RMSD plot, displayed in the same figure, provides an insight to conformational variations occurring during the simulations. RMSD indicates that the ion exit leads to conformational variation. In order to identify the portions of the quadruplex that are most affected, the RMSD was calculated separately for the three main structural elements: loops, sugar-phosphate backbone and guanine quartets (Figure 3, Set 1). The largest variations are observed in the RMSDs of the loops and, to some extent, of

the backbone. The G quartet RMSD is not significantly affected by the ion motion inside the channel. To verify whether the observed ion exit is a probable or a rare event, an independent second simulation was performed starting from the equilibrated system and assigning different initial velocities. Also in this second simulation one K^+ exits from the channel after 10 ns, and differently from that in the first simulation no new ion enters the channel. Also in this second simulation, the escape of the channel ion leads to significant structural changes (Supporting material, Figure S3 and Table S2).

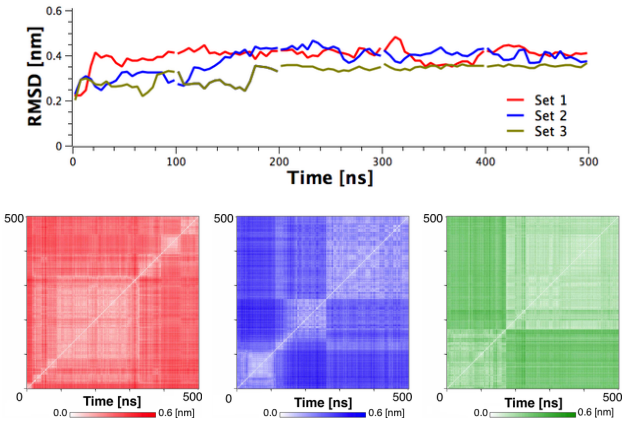

Figure 2: (Top) RMSD of all atom positions starting from the experimental 1KF1 crystal structure for different parameter sets. (Bottom) Representation of the pairwise RMSD: red Set 1; blue Set 2; green Set 3. Deviation is comprised between 0 (white) and 0.6 nm (color).

Set 2: JC ion parameters / TIP3P water model This combination of ion/water parameters has recently been used in MD simulations.[17,36] In contrast to the Set 1 simulations, no ion exit from the quadruplex channel was observed during 500 ns of MD simulation. The channel ion coordination remained close to that in the experimental crystal structure. In the first 140 ns of simulation the RMSDs of the loop are significantly smaller than those observed for parameter Set 1, as shown in Figure 3. However after 150 ns somewhat larger RMSDs are observed for the loops, and to a much lesser extent, also for the backbone, approaching values comparable to those observed for Set 1. Figure 3 shows that the total RMSD increase is due to the loop fluctuations. The larger conformational fluctuations after 150 ns mainly involve reorientations of the loops bases. A similar behavior has been reported by Islam *et*

al.[35] in the study of the same quadruplex but with slightly modified ion parameters. We observe the same conformational variations, characterized by the central thymine in loop 1 moving from one side of the backbone to the other side. After 280 ns of simulation the RMSD of the loops returns closer to the experimental crystal structure (Figure 3, Set 2), and at the same time the pairwise-RMSD indicates a transition into a conformation similar to that observed at 120 ns (Figure 2, blue curve). This transition was due to a large fluctuation in the second loop, as determined by calculating the RMSD of each loop separately (Supporting material, Figure S2).

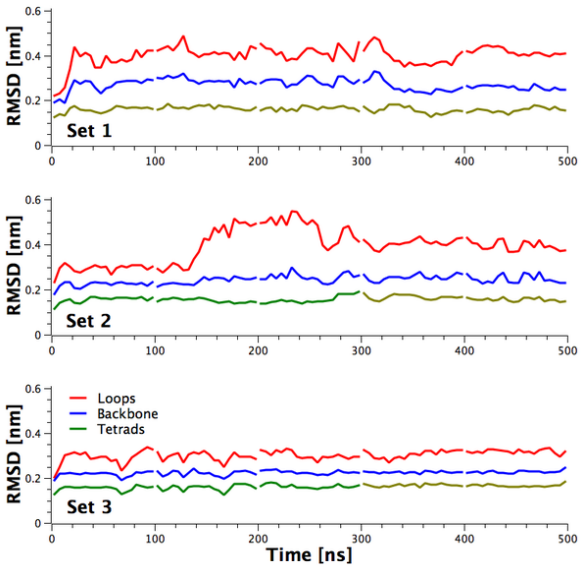

Figure 3: Time evolution of the RMSD of the atomic positions from the experimental 1KF1 crystal structure in the simulation performed with Set 1, Set 2 and Set 3 parameters for separate quadruplex portions.

Set 3: JC Parameters, TIP4P$_{ew}$ Water model To the best of our knowledge, this combination has not been used previously in simulations of quadruplex DNA structures. Compared to the simulations with Set 1 an Set 2, the simulated quadruplex structure deviates less from the experimental one, as can be seen from the RMSDs. In particular, the RMSDs of the loops are significantly lower than those in Set 1 and 2 (Figure 2). As seen from the RMSDs in Figure 2 loops, backbone and quartets do not seem to undergo any large structural

changes during the simulations. The total RMSD in Figure 2 reaches a stable value around 180 *ns*. The corresponding pairwise-RMSD shows two structural clusters during the whole simulation, and the transition to a stable value in the regular RMSD corresponds to a transition between the two clusters. The average of the total RMSD is reported in Table 3 together with the standard deviation. Compared with Set 1 and Set 2, Set 3 has an RMSD lower than 0.5 Å, and also a much lower deviation range, nearly half of that of the other sets. Independent additional simulations for Set 2 and 3 did not show the same difference between the RMSDs. The total RMSDs were lower than those in the first simulation for Set 2, and very similar to those observed for Set 3. However, the standard deviation was again significantly lower for the Set 3 (Supporting material, Table S2).

Table 3: Mean of the RMSD for different simulation sets and their standard deviation values.

RMSD	average *(nm)*	σ *(nm)*
Set 1	0.407	$\pm$ 0.031
Set 2	0.408	$\pm$ 0.029
Set 3	0.349	$\pm$ 0.015

3.1.2 Root mean square fluctuations

In Figure 4 are shown the root mean square fluctuations (RMSF) of atomic positions with respect to the crystal structure of the studied quadruplex. Analysis of Sets 1 and 2 reveals that, despite the fact that all the three loops have an identical sequence and are all of the propeller type, the loops 1 and 2 undergo much larger fluctuations than loop 3. In addition, also the relative intensity of the RMSF varies with the loop; *e.g.* in Set 1 the second thymine shows smaller fluctuations than the adenine in the first loop, while the opposite is true for the second loop. The difference between the fluctuations among the loops is much less pronounced in Set 3 simulations: the loop geometry is kept close to that in the crystal structure during the whole run. Also the RMSFs for residues not belonging to loop 1 and 2

are slightly lower with Set 3 compared to other Sets. Although the analysis of the RMSD and RMSF provide useful information about structural changes, more specific descriptors are needed to analyze the impact on the structure of different parameter sets in simulations. [59] In order to investigate the quadruplex structural dynamics in more details, we have calculated additional properties such as the radial and spatial distribution functions of ions and water molecules around the quadruplex and analysed the trajectories of all torsion angles.

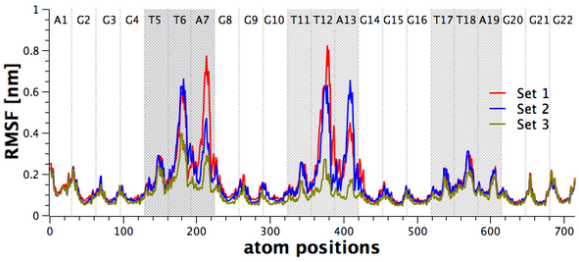

Figure 4: RMSF of atomic positions from the reference experimental 1KF1 crystal structure for different parameter sets.

3.1.3 Radial distribution functions

In Figure 5 we report the radial distribution functions (RDFs) between the sugar-phosphate moieties constituting the backbone (B) or the nucleobases guanine (Gu), adenine (Ad), thymine (Th), and the counterions outside the channel (K), between K with itself, and between counter ions in the channel (Kin) and counter ions outside of the channel. The figure clearly shows that with different sets of parameters the Gu-K, B-K and Th-K distributions do not only change quantitatively but also qualitatively. Indeed, the relative maxima of the first and second peak in the B-K distributions have the opposite behaviour for Set 1 compared to that in the other two sets. The highest peaks are observed for Set 3, and this is accompanied by reduced structural fluctuations and smaller deviation from the experimental structure, as indicated by the RMSF and RMSD. RDFs alone cannot give a complete picture of the three-dimensional distribution of the ions around the molecule, while it can be obtained in the spatial distribution functions (SDFs).

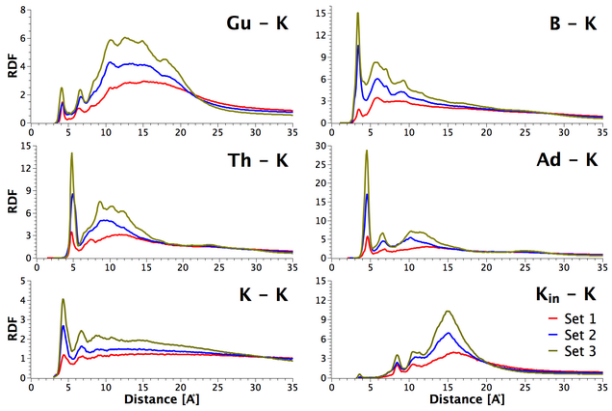

Figure 5: RDFs for selected combinations between guanine nucleobase bead (Gu), Backbone deoxyribose-phosphate group bead (B), thymine nucleobase bead (Th), adenine nucleobase bead (Ad), potassium outside of ion channel (K) and potassium inside of ion channel (Kin). RDF between beads are calculated as the RDF of the center of mass of the atoms in each bead.

3.1.4 Spatial distribution functions

Spatial distribution functions are extremely useful tools to visualize the interactions between the ions and the quadruplex, and can be of help also in the interpretation of the corresponding RDFs. The SDFs are shown in Figure 6, using the same iso-density value for all sets. Even at a first glance, the figure clearly shows a marked difference in the ion affinity to the quadruplex surface, which increases from Set 1 to Set 2 and even further in Set 3, as already indicated by the relative intensities of the peaks of the three sets in the RDFs.

In the SDF of Set 1, besides the two peaks of potassium density corresponding to the two ions in the channel, only another high density region is observed near N3 and O4' of G7, forming a bridge with A13. No regions with high ion densities are observed near the backbone. Considering that the loop backbone is flexible, this lack of high-probability regions could be due to this internal motion preventing to fix the local frame for the SDFs. However, we can exclude that this is the case on the basis of the RDF between backbone beads and cations (B-K), which do not show any high peaks close to this part of quadruplex (Figure 5). In the SDF of Set 2 several regions of high probability of ion occupation can be clearly seen near the loops, the grooves, and also near guanine. In particular, as seen schematically in

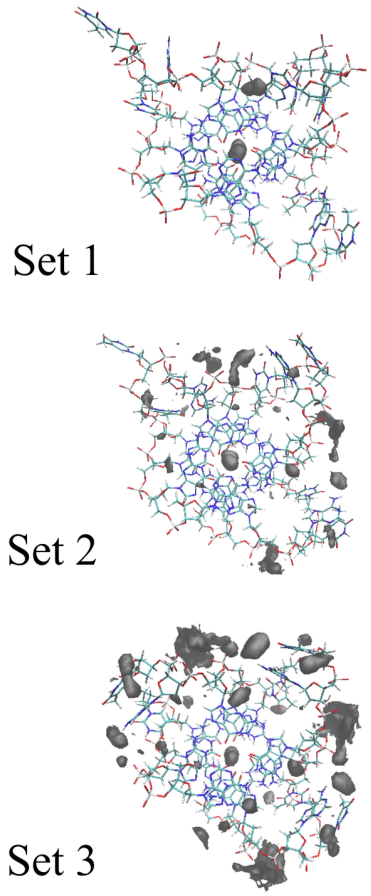

Figure 6: SDFs of potassium around the averaged quadruplex structure at 0 mM KCl concentration. The same threshold value (iso-value 300) is applied for all sets. The Loop 1 is on the top left, and Loop 2 and 3 follow clockwise. The contour level corresponds to $1.8{\cdot}10^{-2}$ K^+ ions / $Å^3$.

Figure 7, the ions are mainly localized near the phosphates; indeed, a rather high first peak is observed in the corresponding RDF. High density is also observed near N3 and O4' of G2 and G14 at a close distance indicating a direct contact, and also near the nitrogen atoms of the adenine base, and oxygen atoms of thymine. Other peaks are observed in the two grooves, between the phosphates of loops 2 and 3 (12, 13, 14 and 18, 19 and 20 respectively in Figure 5 and to a lesser extent in loop 1, where they are organized in a slightly different way than in the other two loops. This difference can be correlated with a different conformation adapted by loop 1 which deviates largely from its initial conformation as it can be seen from the RMSD calculated for the three loops separately (Supporting material, Figure S2). Small regions with a high probability of finding the ions are found also near the phosphates 4, 10 and 16, however on the overall it can be concluded that near the adenine side of the loops there is a higher probability of finding a coordinate ion. The SDF for Set 3 reveals a larger network of interactions between the counter ions and the quadruplex. Differently from what was observed for Set 2, where the loop regions have different distributions, the ion SDF is very similar in the three loops. Considering also the increased probability of finding the ions near the core and loop region revealed by the RDF in Figure 5 we can conclude that this combination of parameters is the one with highest affinity overall between DNA and K^+.

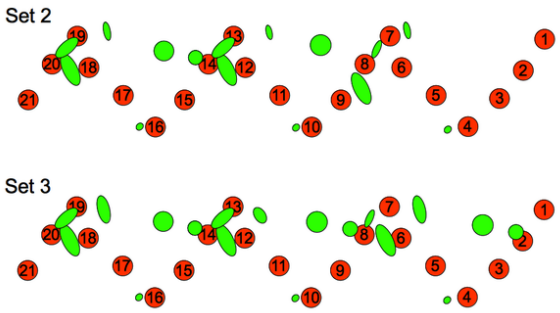

Figure 7: Schematic representation of the interactions between K^+ and the backbone phosphates in the Set 2 and Set 3 MD with minimal salt conditions.

3.1.5 Torsion angles

In comparison with canonical duplex DNA, the torsion angles of human telomeric quadruplexes are quite different due to conformational restrictions imposed by the system topology in these structures; their sampling can serve as a good validator for the used force fields.[17,35] Regarding the loops, it has been recently shown by Collie *et al.*[60], that the most frequent topology of human telomeric TTA loops in available X-ray DNA quadruplexes does have a native arrangement of loops corresponding to that of the 1KF1 quadruplex crystal structure, termed as type 1. For instance, in the 5' $\rightarrow$ 3' direction, the α/γ torsion angles of the first thymine in each loop were found in g+/t, second thymine in t/g+ and the third adenine in g-/g+ conformations,[10] as can be seen in the first column of Figure 8, where the torsion angles for the crystal structure are given (t $\approx 180^\circ$, g+ $\approx 60^\circ$ and g- $\approx 300^\circ$).

The three simulations Sets employed in the present investigation, share the same force field for DNA.[19] Therefore, some known limitations of the force field concerning the loops have been inherited here. The known rearrangement of loop parts which included an early backbone flip of T5, T11, T17 thymines α/γ torsion angles into the 240°/g+ values is due to the force field backbone corrections (necessary for canonical DNA). The adenine interactions with the thymines in the loops are observed to be slightly different from what is observed in the crystal structure with the adenine stacking with the flanking thymine instead that with the first thymine of the loop. These differences between the modeled and the crystal structure have already been described and discussed by Fadrná *et al.*[17] We have computed the time distribution of all torsion angles in each loop residue during the MD simulations for three parameter sets, as described in the Methods section. The obtained distributions have been subsequently clustered with resolution of 15° and afterwards normalized, which provided us an angle fluctuation rate in percent. All torsion angles in each residue of the 1KF1 quadruplex loops, together with the values in the crystal structure, are shown in the compact wheel representation in Figure 8. Comparison of the torsion angles obtained with different Sets indicates that their behaviour is affected by the combination of the different

parameters.

The Set 1 torsion angles of the loops indicate different conformations in comparison with the crystal structure (probably as a consequence of the above discussed escape of the K^+ ion from the channel at the beginning of simulation). The first two loops deviate largely from the crystallographic structure, as shown in the second column of Figure 8. The torsion angles span over a wide number of possible angle clusters (in some cases even covering them all, e.g. the χ torsion angle of A13 residue), suggesting many different loop geometries for this set. Moreover, some of torsion angles were stabilized to non-crystallographic values, as the ϵ torsion angle of T12 residue around 270° for instance. The obvious diversity of torsion angles can clarify previous observations of larger RMSD and RMSF for loop residues and this set. The torsion angles of the the loop residues for Set 2 differs from those observed for Set 1. The range of occupied angle clusters is obviously smaller (increased number of white regions) and the probability to find the torsion angle at a position close to the crystal structure values higher (intensity of red color increased), the third column of Figure 8. Nevertheless, some values still do not correspond to their experimental data. For instance from the first loop, the T6 residue ζ torsion angle is found around 90° or the A7 residue ϵ around 200°. Even here we can refer to the previously discussed larger RMSD and RMSF with observed diversion of torsion angles from crystal structure values. The last column of Figure 8, corresponding to the Set 3, were found closest to the crystal structure. The all three loops clearly prefer a certain combination of similar torsion angles with increased probability, corresponding to values comparable with experimental data. This combination of torsion angles can be linked with the above discussed loop 1 type arrangement[60]. Note, that the crystal α/γ torsion angles of the first loop thymine changed completely during the MD simulations due to used force field even in this case. However, the used set of parameters improved the stability of the torsion angles for all three loops in comparison with crystallographic data, resulting in a folded loop geometry in general.

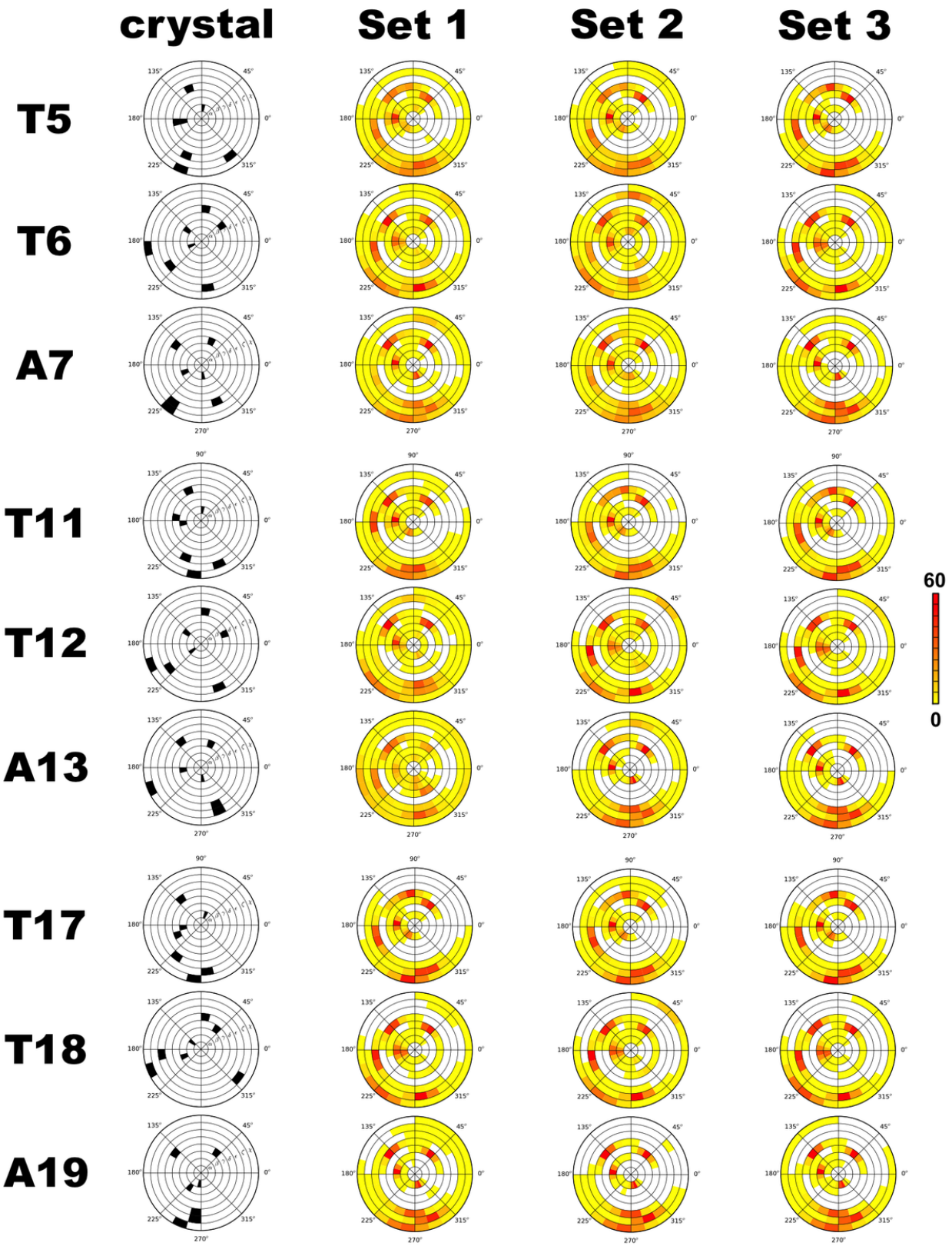

Figure 8: Comparison of all torsion angles in a wheel representation (angle fluctuation rate, values clustered with resolution of 15°). The single wheel represents a torsion angle probability to occur during MD simulation in percent, arranged from α (middle) to χ (edge) torsion respectively. In the four columns are the 1KF1 quadruplex crystal structure and different simulation sets, respectively. In every row are the residues of three quadruplex loops. The white circle cluster spots correspond to angle values which never occurred.

3.2 Simulations at varied ionic strengths

The effect of the ionic strength was evaluated by adding KCl salt into systems of Set 2 and 3, using the JC parameters also for the chloride co-ions Cl^-. The added salt concentration was of 50, 100 and 200 mM, and the corresponding systems are denoted as Set 2_{HC} and Set 3_{HC}, for a comparison also the 0 mM simulation is included in the Figures and Discussion. The Set 1_{HC} combination has also been tested using the Dang[42] parameters for chlorine, but as already observed in previous simulations,[18,40,61] these old default ion parameters did cause KCl to form aggregates; therefore this set will not be further dealt with here.

3.2.1 Root mean square deviations

In figure 9 are reported the all atom RMSDs calculated for the quadruplex structure in Set 2 and Set 3 simulations at different salt concentrations. The RMSDs for each loop are reported in supporting information, Figures S6 and S7. It is interesting to note that by varying the ionic strength the RMSDs quickly reach different plateau values, or in some cases, do not reach any at all, depending on the concentration of the added salt. This is an indication that the salt concentration affects the structure. It is also noteworthy that in both Set 2 and Set 3 the RMSD is the smallest at 50 mM, indicating that small amounts of added salt has a stabilizing effect, while larger concentrations can induce large structural variations. For Set 3, the RMSD increases with the salt concentrations, while the rise of RMSD after 300 ns at 200 mM correspond to higher deviation of loop 1 and loop 3 (Supporting material, Figure S6). The trend is less clear with Set 2, where the RMSD reaches higher values at 100 mM.

3.2.2 Root mean square fluctuations

The RMSFs reported in Figure 10 indicate that in 2_{HC} the fluctuations of the loops vary with the concentration, but no clear trend can be observed. In fact, no large variations are observed in loop 3, while the loop 2 RMSFs are significantly reduced at 50 and even more at 200 mM, but this is not the case for the intermediate concentration of 100 mM. In Set 3,

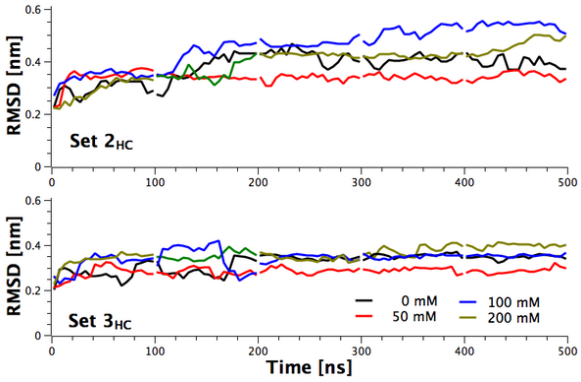

Figure 9: RMSD of the positions of all atoms with respect to the reference experimental 1KF1 crystal structure for Set 2_{HC} and Set 3_{HC}.

the fluctuations slightly decrease increasing the concentration up to 100 mM; however with a further increase in concentration the first and third loop have a much larger RMSF. On the overall the data indicates that the structure becomes less flexible at high salt concentrations, but, as it will be discussed in sub-section 3.2.5 high concentration of salt can stabilize different conformations, and also this phenomenon leads to an increase in the RMSF.

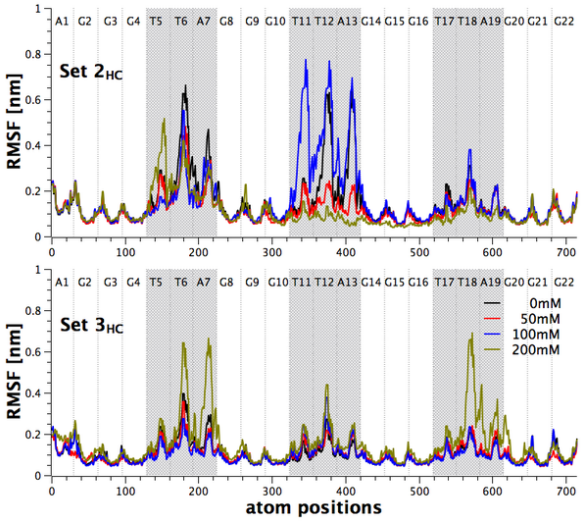

Figure 10: RMSFs of atomic positions with respect to the reference experimental 1KF1 crystal structure for Set 2_{HC} and Set 3_{HC}.

3.2.3 Radial distribution functions

The RDFs of the counter ions with respect to the selected atoms of the quadruplex and the ions in the channel are reported in Figure 11. It is noteworthy to remind that since ion bulk concentration increases with the amount of added salt, it is to be expected that the intensity of the normalized RDF peaks decreases with the added salt and that for a quantitative comparison, which is not of particular interest here, the integral of the RDFs peak should be considered instead. The RDFs indicate that the ion interactions with the quadruplex are qualitatively similar at varying concentration, with three notable exceptions. (1) Set 2 at 100 mM added salt concentration has a much higher peak at direct contact with guanines. (2) Set 2 at 200 mM has much higher direct contact with adenine, and (3) Set 3 at 50 mM has a rather high peak at about 4 Å with the channel potassium.

3.2.4 Spatial distribution functions

In Figures 12 and 13 are displayed the SDFs calculated from the trajectories obtained using the Set 2 and Set 3 parameters, respectively.

Set $\mathbf{2}_{HC}$ At 50 mM the SDFs are very similar to those observed at 0 mM, with no high probability near the first loop, and with the same regions of high density already described for 0 mM near loops 2 and 3. At higher added salt concentrations some differences in the SDFs are observed with high probability regions near loop 1 (Supporting material, Figure S7) and inside of loop 2, in direct contact with G9. On the other side of loop 2 and near loop 3 the high probability regions are similar to those observed at 0 and 50 mM. At 200 mM the SDFs are different, and no clear resemblance to the 0 mM distribution is observed; this difference is also due to the structural deformation of the quadruplex at this concentration, as it can be observed in the average structure shown in Figure 12.

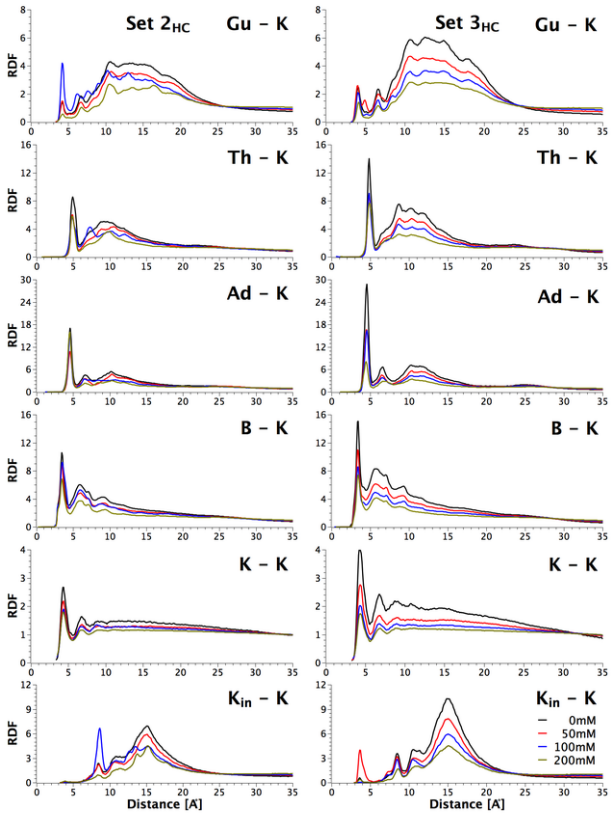

Figure 11: RDFs for Set 2_{HC} (left) and Set 3_{HC} (right) of some combinations between guanine nucleobase bead (Gu), Backbone deoxyribose or phosphate group bead (B), thymine nucleobase bead (Th), adenine nucleobase bead (Ad), potassium outside of ion channel (K) and potassium inside of ion channel (Kin). The bead is defined as the center of mass of all included atoms in the group.

Set 3_{HC} At 50 and 100 mM the main features remain the same as at 0 mM. However, at 50 mM an additional region with a high ion probability appears near the quadruplex channel on the side of A1, which is not stacked over the quadruplex plane (Supporting material, Figure S8). This explains the peak at short distance in the Kin-K RDF in Figure 11. At 200 mM the spatial distribution function maintains the features observed at 0 mM, although the structure is more flexible than at other salt concentration, see sub-section 3.2.2.

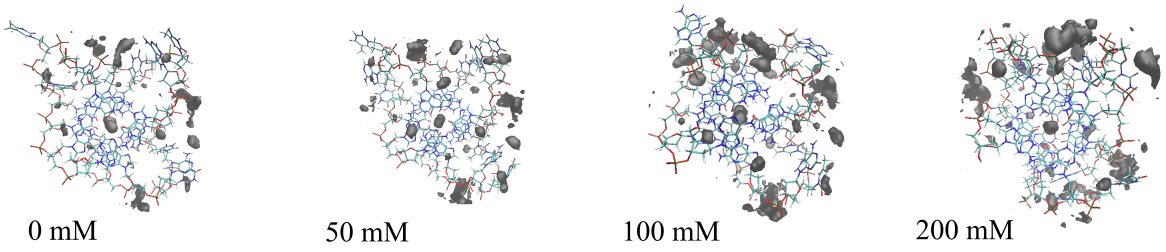

Figure 12: SDFs of potassium around the averaged quadruplex structure for Set 2_{HC}. The Loop 1 is on the top left, and Loops 2 and 3 follow clockwise. The contour level corresponds to $1.8{\cdot}10^{-2}$ K^+ ions / Å^3.

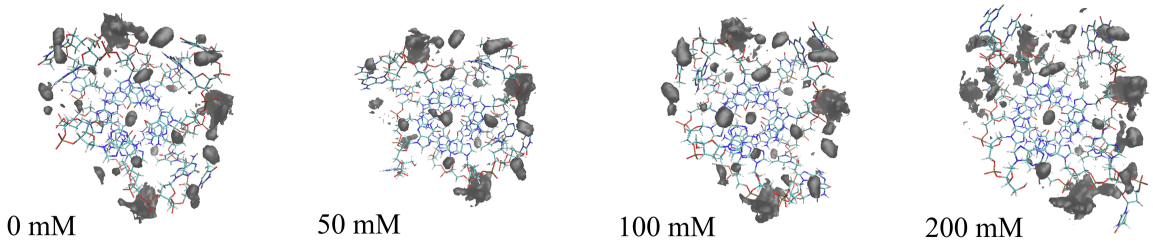

Figure 13: Spatial distribution functions of potassium around the averaged quadruplex structure for Set 3_{HC}. The Loop 1 is on the top left, and Loops 2 and 3 follow clockwise. The contour level corresponds to $1.8{\cdot}10^{-2}$ K^+ ions / Å^3.

3.2.5 Unusual conformations observed with added salt

In the case of Set 2 100mM simulations, a new conformation is observed: the first thymine base of the first loop stacks by a π-π interaction on the guanine G4. The flipping to this position occurs after about 120 ns, and is kept till the end of the simulation. Such a flipping

is responsible of the sudden increase in the RMSD, as shown by the RMSD in Figure 9 and in Figure S5 in the Supporting Information. The absence of T5 from the side region usually occupied by loops nucleobases, provides an easier access to the counter ions, which can stably bound at the both sides of the loop 1; this is reflected in the RDF between adenine and K^+, which has a relatively high peak between 4 and 5 Å (see Figure 11). In analyzing the normalized RDF, it has to be kept in mind that since the bulk concentration is very different at 0mM and 100 mM of added salt, the same height of the first peak of the RDF indicates much higher concentration of ions in the 100 mM system. The SDF clearly shows a high probability of finding counterions around loop 1 (Supporting material, Figure S7). In addition, a high occupation of counterions is observed in the groove between loop 2 and the backbone of the preceding guanines (G7, G8, G9), as shown by the rather high peak at 4 Å. With the same Set (Set 2), the thymine stacking to the nearby guanine is observed also at 200 mM, and it occurs in another loop (the 2nd) at about 170 *ns*. Also in this case the RMSD reflect the structural variation as shown in Figure 9 and in Figure S5. As observed for the similar conformation at 100 mM, the thymine stacking on the top of the G-quartet, allows more ions to interact with the remaining bases (adenine) in the loop, and this is reflected in the RDF in Figure 11. However, in this case, the RDF do not indicate any increase in the ion contact with guanine. It is possible that longer simulation time is required to sample such interactions.

4 Conclusions

Simulations performed with different combinations of water models and ion parameters produce significantly different results concerning the stability of the entire structure, the dynamics of the loops, the interactions with counterions either at minimal salt conditions or in presence of added salts.

Ions in the channel. Using the widely employed combination of Åqvist parameters

for K^+, the TIP3P water model, and the parmbsc0 force field for DNA, one of the two ions in the channel exited inducing a significant structural modification. Although the quadruplex was capable to incorporate a new ion in the channel after some time, such fast ion exchange is not in agreement with time-scales of ion exchanges typical for quadruplexes.[31,62–64] Note that similar ion instability has also been reported in simulations of quadruplexes with CHARMM force field.[65,66] With the same DNA force field, using the Joung and Cheatham parameters either with TIP3P and TIP4P$_{ew}$ water model no ion exits from the channel were observed in a total of 5 μs simulations.

Structure and dynamics of the loops. Performing the simulation at the minimal salt condition using the TIP3P water model shows a pronounced difference in the mobility among the three loops, as shown by the RMSD and its standard deviation. Simulation performed with the Joung and Cheatham ion parameters and the TIP4P$_{ew}$ water shows considerably lower standard deviation of RMSD in all simulations. Moreover, the investigated torsion angles remain closer to the experimental structure with the same Set (Set 3).

Ion affinity. The ion affinity for the quadruplex varies largely with the used ion parameter/water models. As observed in previous investigations with duplex DNA[25] the Cheatham parameters lead to a higher affinity of the counter ions to DNA, and the largest affinity is observed with the TIP4P$_{ew}$ water model.

Effect of the ionic strength. Addition of a small amount (50 mM) of KCl with both Set 2 and Set 3 leads to smaller structural fluctuations. Further addition of salt has a different effect depending on the used potential parameter set. Simulations performed with Set 2 after adding 100 or 200 mM of KCl caused an important structural modification, with the loops adopting conformations not reported in previous simulations, or experimentally. In both cases the first thymine of the loop gets stacked on the top of the quadruplex, leading to a reduction of the flexibility of the loops accompanied

by variation in the conformation of the nearby loop(s) altering the interactions with the counter ions. Using the Joung and Cheatham parameters and the TIP4P$_{ew}$ water model, the addition of salt up to 100 mM leads to a reduction of the mobility of the loops, while at the 200 mM salt concentration the fluctuations of the loops and their RMSD are enhanced. On the overall the results indicate that the simulations performed with Set 3 maintain the quadruplex structure closer to the crystal structure compared to Set 2. However, in all cases high salt concentration leads to an increase in the fluctuations, and this induces unusual conformations with Set 2.

Furthermore, the difference in the average behaviour observed in separate half microsecond long simulations indicates that a proper sampling on the conformational space requires very long simulations. This is in agreement with what was observed previously by Islam *et al.* and it is an important information for developing a bottom-up coarse-grained model of these structures from atomistic simulation. Indeed, extended structure, such as those of compact multi-quadruplex structures[67,68] or those of continuously stacked G-tetrads which could be used to construct biological nanowires,[69] are too large to be amenable by atomistic simulations. A natural way to overcome current computational limitations of atomistic simulations is to use coarse-grained (CG) models to accelerate the simulations by lowering the resolution of the system using its simplified representation. Usually the CG models are built on the base of results of atomistic trajectory,[70,71] therefore CG representation inherits the information from the underlying detailed model (including artefacts). In other words, the CG model is only as good as its atomistic template. For these highly charged polymers the interaction with counterions are of great importance and the cross check of atomistic simulations constitute an important part of the results validation.

Supporting Information Available

Additional RMSD/F data for different simulation Sets, different quadruplex portions (loop 1, 2, 3), different KCl concentrations; key simulation data from the auxiliary run, SDFs

calculated from two specific events (see the main text) and the description of the mechanism of the observed ion exchange for Set 1 (see the main text). This material is available free of charge via the Internet at `http://pubs.acs.org/`.

Acknowledgement

The research leading to these results has received funding from the European Community's Seventh Framework Programme (FP7-REGPOT-2012-2013-1) under grant agreement 316310 CELIM "Fostering excellence in multiscale imaging". A.L. wishes to acknowledge the Swedish Research Council (VR) for financial support. F.M. gratefully acknowledge financial support from the Regione Autonoma della Sardegna, through the Legge Regionale 07/09/2007 (code CRP-59740) and Prof. Giuseppe Saba for technical support. J.S. was supported by the Czech Science Foundation grant 16-13721S and by the project CEITEC 2020 (LQ1601) with financial support from the Ministry of Education, Youth and Sports of the Czech Republic under the National Sustainability Programme II. A.L. gratefully acknowledges the Visiting Professor Programme financed by the Regione Autonoma Sardegna. M.R. was supported by the VVGS-2014-153 project. All authors acknowledge the Swedish National Infrastructure for Computing (SNIC).

References

(1) Wright, W.; Tesmer, V.; Huffman, K.; Levene, S.; Shay, J. Normal Human Chromosomes Have Long G-Rich Telomeric Overhangs at One End. *Genes Dev.* **1997**, *11*, 2801–2809.

(2) Biffi, G.; Tannahill, D.; McCafferty, J.; Balasubramanian, S. Quantitative visualization of DNA G-quadruplex structures in human cells. *Nat. Chem.* **2013**, *5*, 182–186.

(3) Maizels, N.; Gray, L. The G4 Genome. *PLoS Genet.* **2013**, *9*.

(4) Maizels, N. G4 associated human diseases. *EMBO Rep.* **2015**, *16*, 910–922.

(5) Hoffmann, R.; Moshkin, Y.; Mouton, S.; Grzeschik, N.; Kalicharan, R.; Kuipers, J.; Wolters, A.; Nishida, K.; Romashchenko, A.; Postberg, J.; et al., Guanine quadruplex structures localize to heterochromatin. *Nucleic Acids Res.* **2016**, *44*, 152–163.

(6) Simonsson, T. G-Quadruplex DNA Structures Variations on a Theme. *J. Biol. Chem.* **2001**, *382*, 621–628.

(7) Neidle, S.; Parkinson, G. The Structure of Telomeric DNA. *Curr. Opin. Struct. Biol.* **2003**, *13*, 275–283.

(8) Davis, J. G-Quartets 40 Years Later: From 5-GMP to Molecular Biology and Supramolecular Chemistry. *Angew. Chem., Int. Ed.* **2004**, *43*, 668–698.

(9) Karsisiotis, A.; Kane, C.; Silva, M. DNA quadruplex folding formalism âĂŞ A tutorial on quadruplex topologies. *Methods* **2013**, *64*, 28–35, Nucleic Acid Struct.

(10) Parkinson, G.; Lee, M.; Neidle, S. Crystal Structure of Parallel Quadruplexes from Human Telomeric DNA. *Nature* **2002**, *417*, 876–880.

(11) Wang, Y.; Patel, D. Solution Structure of the Human Telomeric Repeat d[AG3(T2AG3)3] G-Tetraplex. *Structure* **1993**, *1*, 263–282.

(12) Dai, J.; Punchihewa, C.; Ambrus, A.; Chen, D.; Jones, R.; Yang, D. Structure of the Intramolecular Human Telomeric G-Quadruplex in Potassium Solution: A Novel Adenine Triple Formation. *Nucleic Acids Res.* **2007**, *35*, 2440–2450.

(13) Chung, W.; Heddi, B.; Schmitt, E.; Lim, K.; Mechulam, Y.; Phan, A. Structure of a left-handed DNA G-quadruplex. *Proc. Natl. Acad. Sci.* **2015**, *112*, 2729–2733.

(14) Cornell, W.; Cieplak, P.; Bayly, C.; Gould, I.; Merz, K.; Ferguson, D.; Spellmeyer, D.; Fox, T.; Caldwell, J.; Kollman, P. A Second Generation Force Field for the Simulation of Proteins, Nucleic Acids, and Organic Molecules. *J. Am. Chem. Soc.* **1995**, *117*, 5179–5197.

(15) Foloppe, N.; MacKerell, J.; Alexander, D. All-atom empirical force field for nucleic acids: I. Parameter optimization based on small molecule and condensed phase macromolecular target data. *J. Comput. Chem.* **2000**, *21*, 86–104.

(16) Ditzler, M.; Otyepka, M.; Šponer, J.; Walter, N. Molecular Dynamics and Quantum Mechanics of RNA: Conformational and Chemical Change We Can Believe In. *Acc. Chem. Res.* **2010**, *43*, 40–47.

(17) Fadrná, E.; Špačková, N.; Sarzynska, J.; Koča, J.; Orozco, M.; Cheatham, T.; Kulinski, T.; Šponer, J. Single stranded loops of quadruplex DNA as key benchmark for testing nucleic acids force fields. *J. Chem. Theory Comput.* **2009**, *5*, 2514–2530.

(18) Mocci, F.; Laaksonen, A. Insight Into Nucleic Acid Counterion Interactions from Inside Molecular Dynamics Simulations is "Worth it's Salt". *Soft Matter* **2012**, *8*, 9268–9284.

(19) Peréz, A.; Marchán, I.; Svozil, D.; Šponer, J.; Cheatham, T.; Laughton, C.; Orozco, M. Refinement of the AMBER Force Field for Nucleic Acids: Improving the Description of Alpha/Gamma Conformers. *Biophys. J.* **2007**, *92*, 3817–3829.

(20) Jorgensen, W.; Chandrasekhar, J.; Madura, J.; Impey, R.; Klein, M. Comparison of Simple Potential Functions for Simulating Liquid Water. *J. Chem. Phys.* **1983**, *79*, 926–935.

(21) Åqvist, J. Ion-Water Interaction Potentials Derived from Free Energy Perturbation Simulations. *J. Phys. Chem.* **1990**, *94*, 8021.

(22) Gkionis, K.; Kruse, H.; Platts, J.; Mládek, A.; Koča, J.; Šponer, J. Ion Binding to Quadruplex DNA Stems. Comparison of MM and QM Descriptions Reveals Sizable Polarization Effects Not Included in Contemporary Simulations. *J. Chem. Theory Comput.* **2014**, *10*, 1326–1340.

(23) Hazel, P.; Parkinson, G.; Neidle, S. Predictive modelling of topology and loop variations in dimeric DNA quadruplex structures. *Nucleic Acids Res.* **2006**, *34*, 2117–2127.

(24) Chen, A.; Pappu, R. Parameters of Monovalent Ions in the AMBER-99 Forcefield: Assessment of Inaccuracies and Proposed Improvements. *J. Phys. Chem. B* **2007**, *111*, 11884–11887.

(25) Noy, A.; Soteras, I.; Luque, F.; Orozco, M. The impact of monovalent ion force field model in nucleic acids simulations. *Phys. Chem. Chem. Phys.* **2009**, *11*, 10596–10607.

(26) Li, M.; Luo, Q.; Xue, X.; Li, Z. Toward a full structural characterization of G-quadruplex DNA in aqueous solution: Molecular dynamics simulations of four G-quadruplex molecules. *J. Mol. Struct.: THEOCHEM* **2010**, *952*, 96–102.

(27) Li, M.; Zhou, Y.; Luo, Q.; Li, Z. The 3D structures of G-Quadruplexes of HIV-1 integrase inhibitors: molecular dynamics simulations in aqueous solution and in the gas phase. *J. Mol. Model.* **2010**, *16*, 645–657.

(28) Petraccone, L.; Garbett, N.; Chaires, J.; Trent, J. An Integrated Molecular Dynamics (MD) and Experimental Study of Higher Order Human Telomeric Quadruplexes. *Biopolymers* **2010**, *93*, 533–548.

(29) Petraccone, L.; Spink, C.; Trent, J.; Garbett, N.; Mekmaysy, C.; Giancola, C.; Chaires, J. Structure and Stability of Higher-Order Human Telomeric Quadruplexes. *J. Am. Chem. Soc.* **2011**, *133*, 20951–20961.

(30) Cang, X.; Šponer, J.; Cheatham, T. Insight into G-DNA Structural Polymorphism and Folding from Sequence and Loop Connectivity through Free Energy Analysis. *J. Am. Chem. Soc.* **2011**, *133*.

(31) Reshetnikov, R.; Šponer, J.; Rassokhina, O.; Kopylov, A.; Tsvetkov, P.; Makarov, A.;

Golovin, A. Cation binding to 15-TBA quadruplex DNA is a multiple-pathway cation-dependent process. *Nucleic Acids Res.* **2011**, *39*, 9789–9802.

(32) Li, J.; Fu, J.; Wang, J.; Hu, D.; Su, Z.; Jin, X. Molecular dynamic and quantum mechanics study of drug recognition for the extremity of DNA G-quadruplex groove. *Med. Chem. Res.* **2012**, *21*, 4010–4016.

(33) Krepl, M.; Zgarbová, M.; Stadlbauer, P.; Otyepka, M.; Banáš, P.; Koča, J.; Cheatham, T.; Jurečka, P.; Šponer, J. Reference Simulations of Noncanonical Nucleic Acids with Different chi Variants of the AMBER Force Field: Quadruplex DNA, Quadruplex RNA and Z-DNA. *J. Chem. Theory Comput.* **2012**, *8*, 2506–2520.

(34) Zhu, H.; Xiao, S.; Haojun, L. Structural Dynamics of Human Telomeric G-Quadruplex Loops Studied by Molecular Dynamics Simulations. *PloS One* **2013**, *8*, 71380.

(35) Islam, B.; Sgobba, M.; Laughton, C.; Orozco, M.; Šponer, J.; Neidle, S.; Haider, S. Conformation Dynamics of the Human Propeller Telomeric DNA Quadruplex on a Microsecond Time Scale. *Nucleic Acids Res.* **2013**, *41*, 2723–2735.

(36) Song, J.; Ji, C.; Zhang, J. The critical effect of polarization on the dynamical structure of guanine quadruplex DNA. *Phys. Chem. Chem. Phys.* **2013**, *15*, 3846–3854.

(37) Zgarbová, M.; Javier Luque, F.; Šponer, J.; Cheatham, T.; Otyepka, M.; Jurečka, P. Toward Improved Description of DNA Backbone: Revisiting Epsilon and Zeta Torsion Force Field Parameters. *J. Chem. Theory Comput.* **2013**, *9*, 2339–2354.

(38) Adrian, M.; Ang, D.; Lech, C.; Heddi, B.; Nicolas, A.; Phan, A. Structure and Conformational Dynamics of a Stacked Dimeric G-Quadruplex Formed by the Human CEB1 Minisatellite. *J. Am. Chem. Soc.* **2014**, *136*, 6297–6305.

(39) Bergues-Pupo, A.; Arias-Gonzalez, J.; Morón, M.; Fiasconaro, A.; Falo, F. Role of the

central cations in the mechanical unfolding of DNA and RNA G-quadruplexes. *Nucleic Acids Res.* **2015**, *43*, 7638âĂŞ–7647.

(40) Joung, I.; Cheatham, T. Determination of Alkali and Halide Monovalent Ion Parameters for Use in Explicitly Solvated Biomolecular Simulations. *J. Phys. Chem. B* **2008**, *112*, 9020–9041.

(41) Smith, D.; Dang, L. Computer simulations of NaCl association in polarizable water. *J. Chem. Phys.* **1994**, *100*, 3757–3766.

(42) Dang, L.; Kollman, P. Free energy of association of K+: 18-crown-6 complex in water. *J. Phys. Chem.* **1995**, *99*, 55–58.

(43) Berendsen, H.; Grigera, J.; Straatsma, T. The missing term in effective pair potentials. *J. Phys. Chem.* **1987**, *91*, 6269–6271.

(44) Kusalik, P.; Svishchev, I. The spatial structure in liquid water. *Science* **1994**, *265*, 1219–1221.

(45) Mahoney, M.; Jorgensen, W. A five-site model for liquid water and the reproduction of the density anomaly by rigid, nonpolarizable potential functions. *J. Chem. Phys.* **2000**, *112*, 8910–8922.

(46) Horn, H.; Swope, W.; Pitera, J.; Madura, J.; Dick, T.; Hura, G.; Head-Gordon, T. Development of an Improved Four-Site Water Model for Biomolecular Simulations: TIP4P-Ew. *J. Chem. Phys.* **2004**, *120*, 9665–9678.

(47) Kührová, P.; Otyepka, M.; Šponer, J.; Banáš, P. Are waters around RNA more than just a solvent? - An insight from molecular dynamics simulations. *J. Chem. Theory Comput.* **2014**, *10*, 401–411.

(48) Berendsen, H.; van der Spoel, D.; van Drunen, R. GROMACS: A message passing

parallel molecular dynamics implementation. *Comput. Phys. Commun.* **1995**, *91*, 43–56.

(49) Lindahl, E.; Hess, B.; van der Spoel, D. GROMACS 3.0: A package for molecular simulation and trajectory analysis. *J. Mol. Model.* **2001**, *7*, 306–317.

(50) Pronk, S.; Pall, S.; Schulz, R.; Larsson, P.; Bjelkmar, P.; Apostolov, R.; Shirts, M.; Smith, J.; Kasson, P.; van der Spoel, D.; et al., GROMACS 4.5: A High-Throughput and Highly Parallel Open Source Molecular Simulation Toolkit. *Bioinformatics* **2013**, *29*, 845–854.

(51) Bussi, G.; Donadio, D.; Parrinello, M. Canonical Sampling Through Velocity Rescaling. *J. Chem. Phys.* **2007**, *126*, 014101.

(52) Hess, B.; Bekker, H.; Berendsen, H.; Fraaije, J. LINCS: A Linear Constraint Solver for Molecular Simulations. *J. Comput. Chem.* **1997**, *18*, 1463–1472.

(53) Darden, T.; York, D.; Pedersen, L. Particle Mesh Ewald - An n.log(n) Method for Ewald Sums in Large Systems. *J. Comput. Chem.* **1993**, *98*, 10089–10092.

(54) Parrinello, M.; Rahman, A. Polymorphic transitions in single crystals: A new molecular dynamics method. *J. Appl. Phys.* **1981**, *52*, 7182âĂŞ–7190.

(55) Nosé, S.; Klein, M. L. Constant pressure molecular dynamics for molecular systems. *Mol. Phys.* **1983**, *50*, 1055âĂŞ–1076.

(56) Mirzoev, A.; Lyubartsev, A. MagiC: Software Package for Multiscale Modeling. *J. Chem. Theory Comput.* **2013**, *9*, 1512–1520.

(57) Kumar, R.; Grubmuller, H. Do X3dna: a tool to analyze structural fluctuations of dsDNA or dsRNA from molecular dynamics simulations. *Bioinformatics* **2015**, *31*, 2583–2585.

(58) Humphrey, W.; Dalke, A.; Schulten, K. VMD - Visual Molecular Dynamics. *J. Mol. Graphics* **1996**, *14*, 33–38.

(59) Bottaro, S.; Di Palma, F.; Bussi, G. The role of nucleobase interactions in RNA structure and dynamics. *Nucleic Acids Res.* **2014**,

(60) Collie, G.; Campbell, N.; Neidle, S. Loop flexibility in human telomeric quadruplex small-molecule complexes. *Nucleic Acids Res.* **2015**, *43*, 4785–4799.

(61) Auffinger, P.; T.E., C.; ; Vaiana, A. Spontaneous Formation of KCl Aggregates in Biomolecular Simulations: A Force Field Issue? *J. Chem. Theory Comput.* **2007**, *3*, 1851–1859.

(62) Deng, H.; Braunlin, W. Kinetics of Sodium Ion Binding to DNA Quadruplexes. *J. Mol. Biol.* **1996**, *255*, 476–483.

(63) Engelhart, A.; Plavec, J.; Persil, O.; Hud, N. *Metal Ion Interactions with G-Quadruplex Structures*; RSC Biomolecular Sciences, 2009; Chapter 4, pp 118–153.

(64) Largy, E.; Mergny, J.; Gabelica, V. *Role of Alkali Metal Ions in G-Quadruplex Nucleic Acid Structure and Stability*; Springer, 2016; Vol. 16; pp 203–258.

(65) Šponer, J.; Cang, X.; Cheatham, T. Molecular dynamics simulations of G-DNA and perspectives on the simulation of nucleic acid structures. *Methods* **2012**, *57*, 25–39.

(66) Ray, A.; Panigrahi, S.; Bhattacharyya, D. A comparison of four different conformations adopted by human telomeric G-quadruplex using computer simulations. *Biopolymers* **2016**, *105*, 83–99.

(67) Vorlíčková, M.; Chládková, J.; Kejnovská, I.; Fialová, M.; Kypr, J. Guanine Tetraplex Topology of Human Telomere DNA is Governed by the Number of (TTAGGG) Repeats. *Nucleic Acids Res.* **2005**, *33*, 5851–5860.

(68) Renciuk, D.; Kejnovska, I.; Skolakova, P.; Bednarova, K.; Motlova, J.; Vorlickova, M. Arrangements of Human Telomere DNA Quadruplex in Physiologically Relevant K+ Solutions. *Nucleic Acids Res.* **2009**, *37*, 6625–6634.

(69) Borovok, N.; Molotsky, T.; Ghabboun, J.; Porath, D.; Kotlyar, A. Efficient Procedure of Preparation and Properties of Long Uniform G4-DNA Nanowires. *Anal. Biochem.* **2008**, *374*, 71–78.

(70) Rebič, M.; Mocci, F.; Laaksonen, A.; Uličný, J. Multiscale Simulations of Human Telomeric G-Quadruplex DNA. *J. Phys. Chem. B* **2015**, *119*, 105–113.

(71) Lyubartsev, A.; Naômé, A.; Vercauteren, D.; Laaksonen, A. Systematic hierarchical coarse-graining with the inverse Monte Carlo method. *J. Chem. Phys.* **2015**, *143*.

Graphical TOC Entry